Supplementary Information for: Experimental Observation of Strong Exciton Effects in Graphene Nanoribbons

Alexander Tries[1,3], Silvio Osella[4], Pengfei Zhang[2], Fugui Xu[2], Charusheela Ramanan[1], Mathias Kläui[3], Yiyong Mai[2], David Beljonne[6] and Hai I. Wang[1,*]

[1]Max Planck Institute for Polymer Research, Ackermannweg 10, D-55128 Mainz, Germany;

[2]School of Chemistry and Chemical Engineering, Frontiers Science Center for Transformative Molecules, Shanghai Jiao Tong University, 800 Dongchuan Road, Shanghai 200240, China;

[3]Institute of Physics and Graduate School of Excellence Materials Science in Mainz, Johannes Gutenberg-University Mainz, Staudingerweg 7, D-55128 Mainz, Germany;

[4]Chemical and Biological Systems Simulation Lab, Centre of New Technologies, University of Warsaw, Banacha 2C, 02-097 Warsaw, Poland;

[6]Laboratory for Chemistry of Novel Materials, Université de Mons, Place du Parc, 20, B-7000 Mons, Belgium.
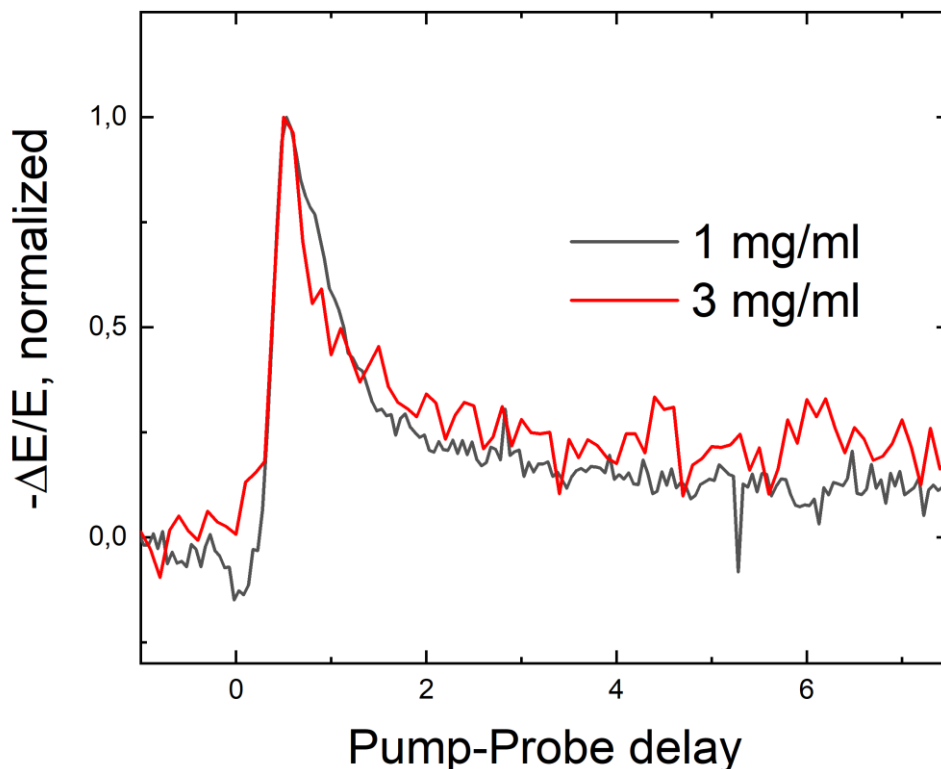
Content

1: Concentration-dependent THz measurements

Figure S1: The Real part of the OPTP conductivity for two different concentrations upon excitation with 3.1eV pump and 100 µJ/cm^2 fluence. No aggregation effects are visible as the dynamics overlap very well.

2: Optical-Pump THz-Probe spectroscopy

The Optical Pump - THz Probe experiments were performed using a commercial, regenerative amplified, mode-locked Ti: sapphire femtosecond laser operating with a central energy of 1.55eV, pulse length of 50 fs and a repeating frequency of 1 kHz. The samples were either pumped with the fundamental laser wavelength, frequency doubled (BiB3O6 crystal) 3.1 eV light or other wavelengths generated with a TOPAS prime NIR - UV/VIS.

A small fraction of the laser output was used to generate single-cycle THz pulses by optical rectification in a 1 mm ZnTe crystal. This leads to ∼ 1 ps THz pulses in the range between 0.4-2 THz. This divergent THz probe pulse was focused onto the sample by using a pair of off-axis parabolic mirrors. After passing through the sample, the THz pulses were subsequently collimated and refocused onto a second ZnTe crystal by a second pair of off-axis parabolic mirrors. By using electro-optic sampling with a third, delayed 1.55 eV detection pulse, the transmitted THz waveform was measured as the temporal evolution of the electric field. By tuning the detection delay, the whole THz probe pulse can be mapped out. Upon repeating this experiment with a varying pump-probe delay, it is possible to map out the temporal evolution of the photoinduced conductivity in THz frequency. For the measurement of the time evolution of the spectrally-weighted, frequency-integrated photoconductivity, the attenuation of the peak THz-probe pulse (real part) or the change of the field in the crossing point of the pulse[42] (imaginary part) is recorded. The pump pulses were delayed with

respect to the THz probe pulse and the polarization of the pump and probe is parallel. The pump beam was chopped at 500 Hz using a mechanical chopper.

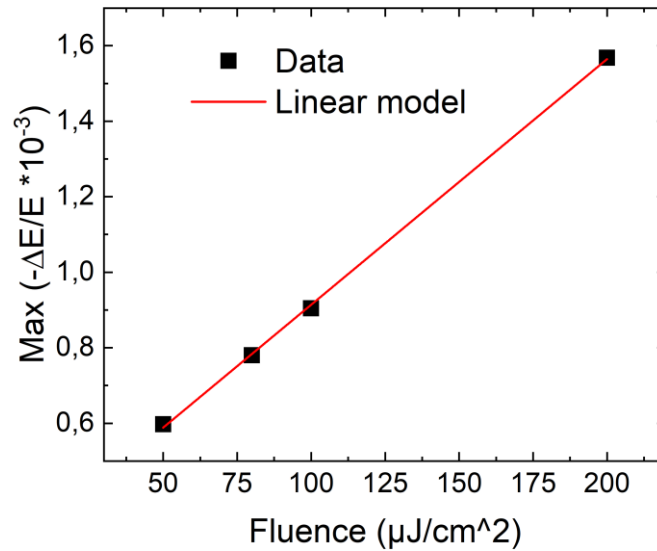## 3: Fluence-dependent THz conductivity maximum

Figure S2: Fluence-dependent THz conductivity maximum upon photoexcitation with 3.1 eV (black dots). The red line represents the linear fitting. The excellent fit to the model indicates that all the THz measurements were performed in a linear regime thus, we can unambiguously rule out any multi-photon excitation effects.
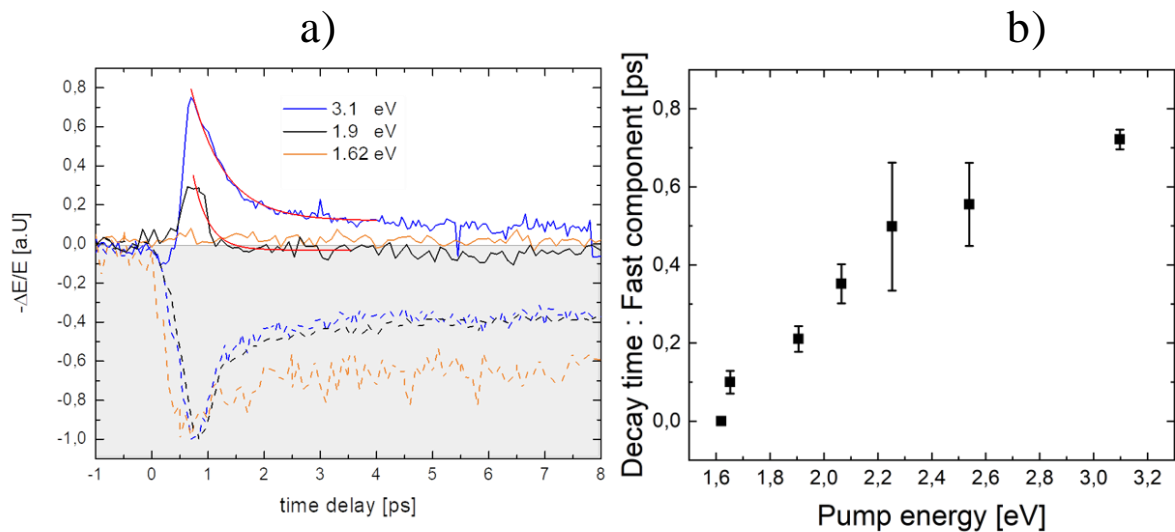
4: Lifetimes of real conductivity

Figure S3: (a) The sub-picosecond time evolution of both the real and imaginary frequency-integrated photoconductivity as a function of the pump-probe delay for three different pump energies (with exponential fittings for the fact decays in the real conductivities) (b) pump energy dependent fast decay time in the dynamics

5: Entropy-driven exciton dissociation

Excitons can be also dissociated into free charges driven by a thermodynamic contribution, e.g. the entropy gain during e-h separation. This implies that the fraction of free charges may consist of two main terms: $\eta_{th}*P_{th}$ (E_B, $h\nu$, T) + $\eta_{entropy}*P_{entropy}$($N$, E_B, T) with E_B as the biding energy, $h\nu$ as the photon energy of the pump, N as the photogenerated carrier density, and T as the temperature and η_{th}, $\eta_{entropy}$ as the relative weight of two contributions, namely the thermal excitation and entropy effect (η_{th} + $\eta_{entropy}$ =100%). As the temperature is fixed at room temperature in our study, we neglect its contribution in the following discussion. The first term for the free carrier generation via thermal excitation, as extensively discussed in our manuscript, is expected to have a sigmoidal-like dependence on the photon energy (or the excess energy) of the pump. The second contribution via entropy-driven free carrier generation, arises from the entropic gain (i.e. and thus lowering the system energy) in the exciton dissociation which is a function of the density and exciton binding energy as described by Saha model[38]. For a fixed excitation density and a given binding energy E_B, the entropy term is expected to display an energy-independent, constant contribution. Hence, if substantial amounts of excitons are dissociated due to the entropy gain, we should have observed a finite real conductivity, even when we resonantly pump the excitonic transition at ~1.63 eV (where the exciton dissociation driven by the thermal fluctuation (the first term) contributes little to the free carrier generation). The fact that we observe ~0% real conductivity, at 1.6-2.2 eV excitations in figure 2a, b, indicates that the dissociation of excitons due to a gain in entropy can be neglected in our study.

More quantitatively, we employ the Saha equation for the 1-dimensional case[38,66] to calculate the free carrier percentage x=$\frac{N_e}{N_{Pump}}$ = $\frac{N_{Pump}-N_{ex}}{N_{Pump}}$ (N_e, N_{ex}, N_{Pump} as the carrier density of free electrons, excitons and initial photogenerated carriers following excitation) as:

$$\frac{x^2}{1-x} = \frac{1}{N_{Pump}} * \left(\frac{2\pi\mu k_B T}{h^2}\right)^{\frac{1}{2}} * e^{-\frac{E_B}{k_B T}} ,$$

in which E_B is the exciton binding energy, μ is the reduced mass of the exciton (approximated to 0.084 m_0 [40]), and h as the plank constant. Plugin in the absorbed photo density ($N_{Pump} = 4.05 * 10^{15} cm^{-2}$) in the equation, one obtains free carrier percentage x ~0%, in line with our discussion.

6: Details on Drude-Smith Fitting

The Drude-Smith (DS) model is a conductivity model, successfully used to describe complex conductivity in semiconducting polymers:

$$\sigma_{DS} = \frac{\varepsilon_0 \omega_p^2 \tau}{1-i\omega\tau} \times \left(1 + \frac{c}{1-i\omega\tau}\right) \text{ (1)}.$$

Here ε_0 is the vacuum permittivity, ω_p the plasma frequency and τ the average scattering time.

The DS model describes the conductivity of free carriers in a medium with a preferential charge carrier backscattering. Hence, it lifts the constraint of the classical Drude model that all the charge carriers scatter isotopically. A preferred direction is introduced by the parameter c, which has values between 0 and -1. For c=0, we come back to the classical Drude conductivity. One key assumption of this model that the preferred backscattering direction is retained for only one scattering event.

Despite this crude assumption, the empirical DS model works remarkably well in describing the conductance of semiconducting polymers.

The plasma frequency is linked to the density of excited charge carriers by

$$\omega_p^2 = \frac{e^2 N}{\varepsilon_0 m^*} \ (2),$$

with e the elemental charge and m^* the effective mass.

In Fig. 4 of the main text, a DS model was fitted to a 2D dataset measured at 0.5 ps after photoexcitation with 3.1 eV. The fit yields to a scattering time of $\tau = 41 \ fs$ and $c = -1$, in well accordance with previous published studies on the THz conductivity of other GNRs.[39,40]

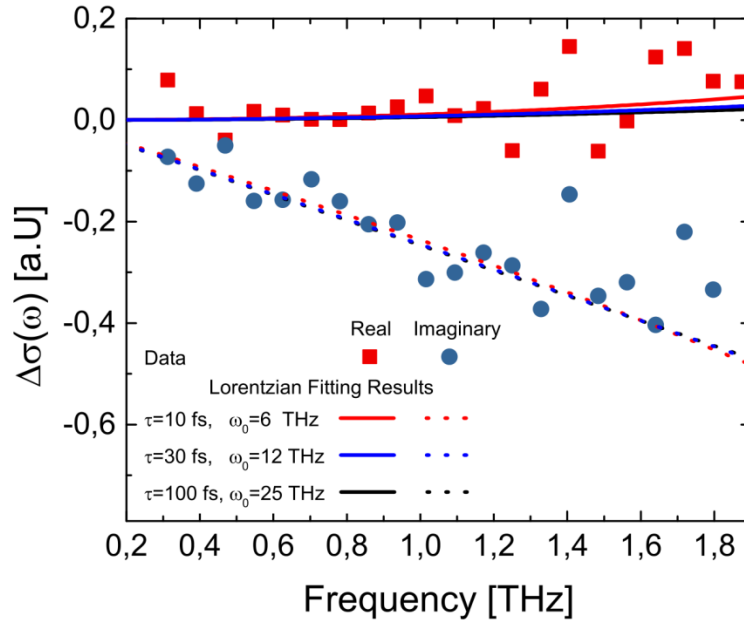## 7: Results of excitonic fitting with a Lorentzian lineshape

Figure S4: The figure shows frequency-resolved real and imaginary photoconductivity as measured with a 1.62 eV pump. Furthermore, it contains three different Lorentzian fittings

Fig. S4 contains frequency-resolved real and imaginary photoconductivity as measured with a 1.62 eV pump. Clearly, we see an almost flat real part as well as a dispersive negative imaginary part. This is a strong hint for an exciton, which is usually modelled by a Lorentzian lineshape with the 1S-1P transition ω_0 and the broadening γ as parameters. Hence, via simple fitting, one could be able to determine these parameters:

$$\sigma(\omega) = \frac{i\omega\varepsilon_0\omega_p^2}{\omega_0^2 - \omega^2 - i\omega\gamma} \ (3)$$

Three fits to this model are shown in Fig. S4. Due to the very large exciton binding energy, the 1S-1P resonance frequency ω_0 will be large as well. Due to the small available bandwidth of the THz-setup, a resonantly measurement scheme is not possible. Hence, a simple fit to a Lorentzian lineshape does not allow for the determination of the binding energy of the GNR as shown in Fig. S5. Several sets of parameters ω_0, γ yield to qualitatively similar fitting results. Therefore, we are not able to determine the exciton binding energy with this approach.

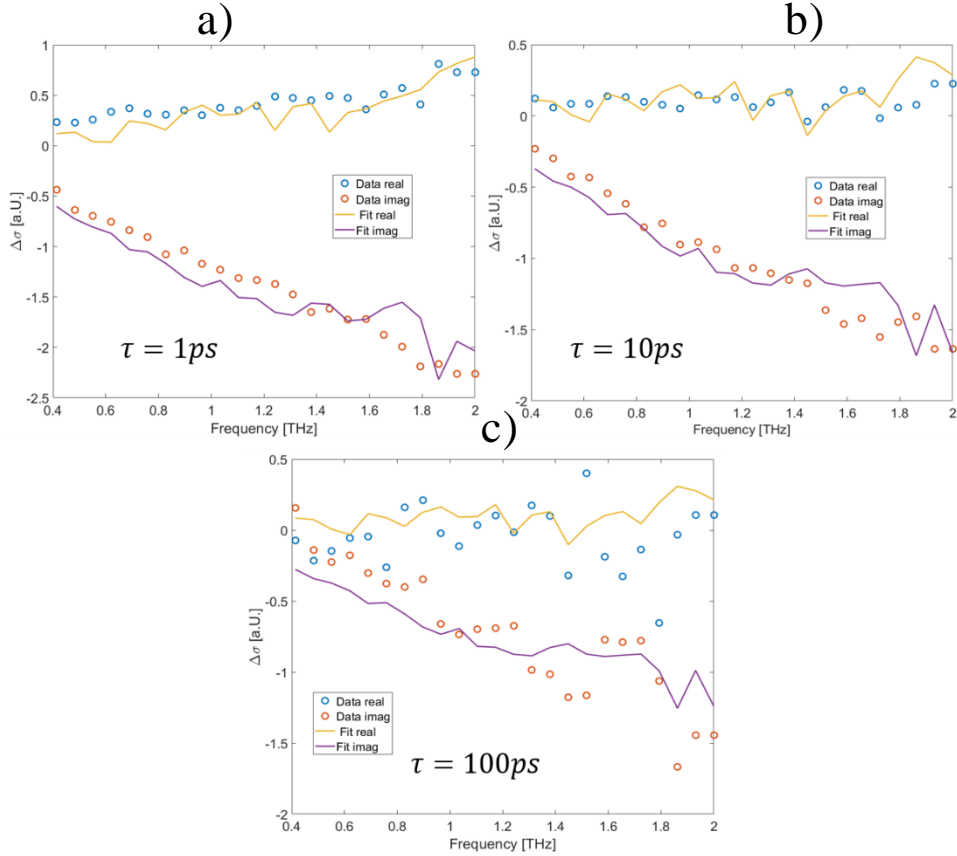## 8: Extraction of exciton formation times and fitting examples

Figure S5: Examples for the fitting results used to extract the exciton formation time. Frequency resolved spectra were measured at a pump energy of 3.1 eV and shown for (a) t=1, (b) 10 and (c) 100 ps after photoexcitation. The fit is a result of a linear superposition between a free-carrier dominant spectrum and an exciton-dominant spectrum as described in the main text.

9: Methods for computation

All computations have been performed with the Gaussian16 software, considering the DFT level of theory and the range-separated screened HSE hybrid functional with the Pople's 6-31G(d) basis set. The geometry of the GNR tetramer has been considered from our previous study.[51] From this structure, a single point energy calculation at the TDDFT level of theory has been performed, in order to study the optical properties of the investigated structure. The analysis of the excited states properties such as partial overlap between the hole and electron transition densities has been performed by the NANCY_EX 2.0 code[62-64] and the quantification of the exciton size with the TheoDORE software.[65]
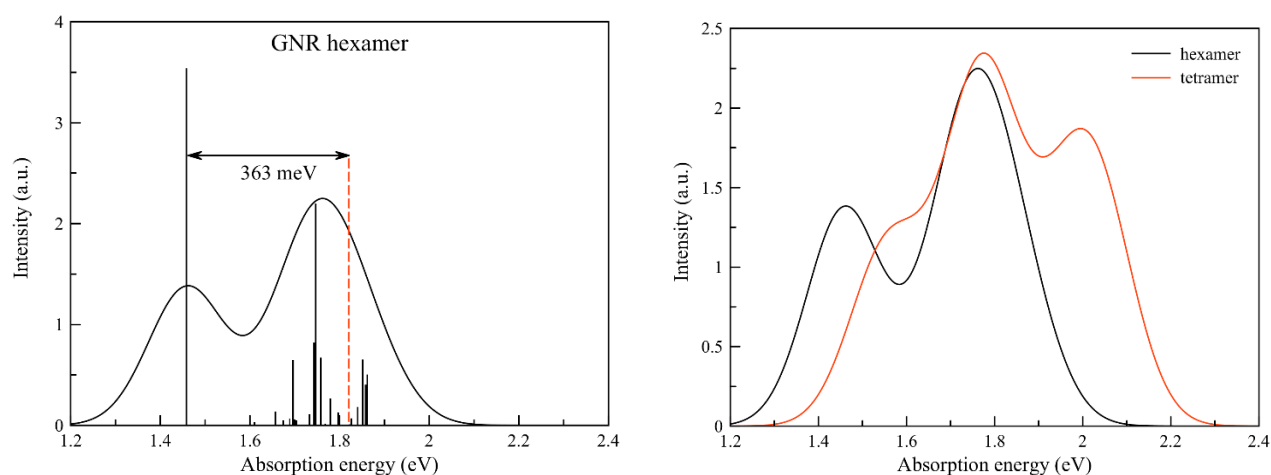
Figures S6: absorption spectrum for the hexamer GNR and overlap of the absorption spectra for both computed oligomers.

In semiconductor theory, it is well established that Frenkel excitons have binding energies in large excess of room temperature thermal energy, in contrast to Wannier excitons. The large exciton binding energies reported in this discussion call for a Frenkel exciton picture. In this view, we performed a quantitative assessment of the exciton size in these ribbons with both experimental and theoretical approaches. This was done using three different models, with results reported in Table T9 below. Model 1 relies completely on experimental data and is based on a kinetic energy analysis. Models 2 and 3 are based on two different computational approaches: the TDDFT method applied in the manuscript (model 2) and a Single Configuration Interaction (SCI) formalism based on the semi-empirical INDO Hamiltonian (model 3). An approximate size for the exciton radius can be obtained by enforcing a Mulliken population analysis to the one-particle transition density matrix provided by TDDFT calculations, see S. Mewes et al.[67] Because it is based on a Zero Differential Overlap (ZDO) approximation, INDO/SCI calculations provide a direct estimate of the exciton average electron-hole separation without further approximation.

Method	Model 1 (exp)	Model 2 (TDDFT)	Model 3 (INDO/SCI)
Exciton binding energy	700 meV	1120 (550) meV	/
Exciton radius	~ 0.7 nm	1.7 nm	0.7 (1.1) nm

Table T9. Experimental and theoretical results for the binding energy and size of the lowest exciton. Calculated data are for a tetramer model and refer to either the gas phase or (between parentheses) include dielectric screening by the medium using toluene parameters as a proxy.

From table T9, there is reasonable agreement between experiment and theory, considering the uncertainty on both set of data. Clearly, the results point towards the formation of strongly bound, Frenkel-like, excitons in the ribbons. Note that the TDDFT calculations are overestimating the exciton size, which is partly related to the self-interaction error only partly cured by using HSE06. Finally, we note that the binding energies and exciton sizes are expected to be sensitive to the screening by the environment. Here, the environment is treated in a continuum model and we considered two limiting cases, the gas phase and the dielectric response of the toluene solvent. Without going to explicit simulations of the medium, one does indeed anticipate the reality to be somewhere in between these two extremes, depending on the extent to which the long alkyl side chains isolate the ribbons from their liquid environment. We stress that the INDO/SCI calculations yield an optical absorption spectrum that is in remarkable agreement with the TDDFT results and the experimental data, see Figure S7.
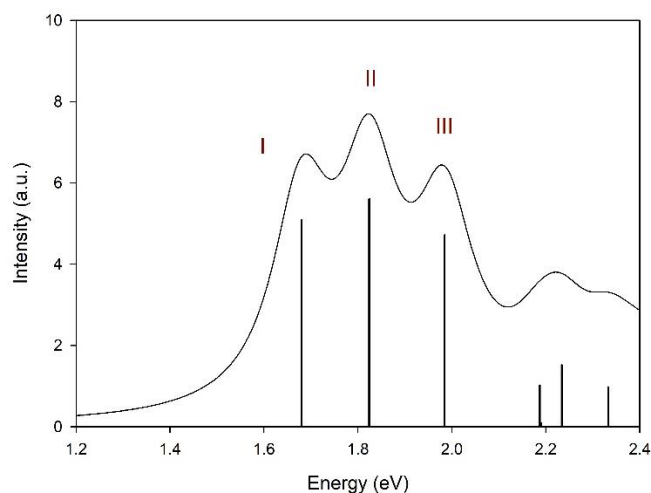

Figures S7: Absorption spectrum for the tetramer GNR computed at the INDO/SCI level of theory, including dielectric screening.
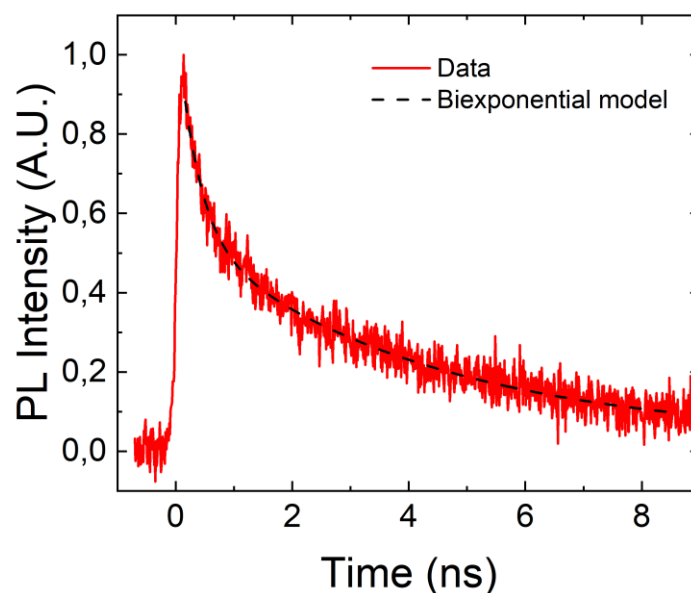
10: Time-dependent photoluminescence

Figure S8: Time-dependent photoluminescence probed at 750nm. The sample was excited by 600nm with fluence of 305 µJ/cm², in the similar range to the fluences used in the THz study. The data can be well described using a biexponential model with a fast decay of $\tau = (0.35 \pm 0.03)ns$ and a slow decay of $\tau = (4.1 \pm 0.3)ns$

Additional references

(62) Etienne, T.; Assfeld, X.; Monari, A. Towards a Quantitative Assessment of Electronic Transitions' Charge-Transfer Character, *JCTC* **2014,** 10, 3896.

(63) Etienne, T.; Assfeld, X.; Monari, A. New Insight into the Topology of Excited States through Detachment/Attachment Density Matrices-Based Centroids of Charge, *JCTC* **2014,** 10, 3906.

(64) Etienne, T. Probing the Locality of Excited States with Linear Algebra, *JCTC* **2015**, 11, 1692.

(65) Lu, T.; Chen, F. J. Multiwfn: a multifunctional wavefunction analyzer., *Comput. Chem.* **2012**, 33, 580.

(66) D'Innocenzo, V.; Gracini, G.; Alcicer, J.P.; Srimath, A.R.; Stranks, S.D.; Lee, M.M.; Lanzani, G.; Snaith, H.J.; Petrozza, A. Excitons versus free charges in organo-lead tri-halide perovskites, *Nat. Comm.* **2014**, 5, 3586.

(67) Mewes, S.A.; Mewes, J.M.; Dreuw, A.; Plasser, F. Excitons in poly(para phenylene vinylene): a quantum-chemical perspective based on high-level ab initio calculations *Phys. Chem. Chem. Phys.*, **2016**,18, 2548-2563